Driving Spin Texture in High-Temperature Cuprate Superconductors via Local Structural Fluctuations

Kayla Currier
Lawrence Berkeley National Laboratory
Chiu-Yun Lin
University of California, Berkeley
Kenneth Gotlieb
University of California, Berkeley
Ryo Mori
University of California, Berkeley
Hiroshi Eisaki
AIST
Martin Greven
University of Minnesota https://orcid.org/0000-0002-8055-4358
Alexei Fedorov
Lawrence Berkeley Natinal laboratory https://orcid.org/0000-0003-3510-3117
Zahid Hussain
Lawrence Berkeley National Laboratory
Alessandra Lanzara (ALanzara@lbl.gov)
University of California, Berkeley https://orcid.org/0000-0002-9519-8974

Article

Keywords:

Posted Date: March 30th, 2022

DOI: https://doi.org/10.21203/rs.3.rs-1439382/v1

Driving Spin Texture in High-Temperature Cuprate Superconductors via Local Structural Fluctuations

K. Currier,[1,2,*] C.Y. Lin,[1,2,*] K. Gotlieb,[3,2] R. Mori,[2] H. Eisaki,[4]
M. Greven,[5] A. Fedorov,[6] Z. Hussain,[6] and A. Lanzara[1,2,†]

[1]*Department of Physics, University of California, Berkeley, California 94720, USA*

[2]*Materials Sciences Division, Lawrence Berkeley National Laboratory, Berkeley, California 94720, USA*

[3]*Graduate Group in Applied Science & Technology, University of California, Berkeley, California 94720, USA*

[4]*Electronics and Photonics Research Institute, National Institute of Advanced Industrial Science and Technology, Tsukuba, Ibaraki 305-8568, Japan*

[5]*School of Physics and Astronomy, University of Minnesota, Minneapolis, Minnesota 55455, USA*

[6]*Advanced Light Source, Lawrence Berkeley National Laboratory, Berkeley, California 94720, USA*

(Dated: March 10, 2022)

Abstract

Spin-orbit coupling emerging out of a material's global inversion symmetry breaking has been long known to act as a pair breaking mechanism to the superconducting order parameter. However, when spin-orbit coupling emerges from local inversion symmetry breaking, an unexpected coexistence with superconductivity might occur. Although lattice driven local symmetry breaking is intrinsic to a variety of unconventional superconductors, little is known about its close connection to spin-orbit coupling, and how the combination of the two can impact electronic properties and the microscopic classification of the order parameter. By using high-resolution spin- and angle-resolved photoemission spectroscopy we reveal the presence of a universal momentum-dependent spin texture throughout the hole-doped side of the cuprate phase diagram for the Bi-based family, which becomes negligible on the electron-doped side. We attribute this spin asymmetry to local inversion symmetry breaking induced by local distortions of the CuO octahedra, revealing an interplay between spin-orbit coupling and lattice symmetry. The implication of this connection in steering the ground state properties of cuprate superconductors is discussed, together with the intriguing possibility that it might provide the long missing link to explain the complexity and asymmetry of the cuprate phase diagram.

* These authors contributed equally to the preparation of this manuscript.

† alanzara@lbl.gov

Symmetry and symmetry breaking are arguably among the most fundamental concepts in physics and more generally are key to classifying and understanding a variety of natural phenomena [1]. The properties of materials can be linked to their various global symmetries, including time and space inversion symmetry. When symmetry is broken in crystals new patterns emerge that give rise to novel phases and properties [2]. For instance, the removal of inversion symmetry can lead to coupling of the electron's orbital motion with its spin, also known as spin-orbit coupling (SOC), eventually resulting in two spin-split electronic bands in momentum.

The ramification of global inversion symmetry breaking in the context of superconductivity has been a matter of study for long time [3, 4], with main consequences on the pairing symmetry via singlet-triplet mixing, and with the general understanding that spin-orbit coupling mostly behaves as a symmetry breaking field to the superconducting state [5, 6]. However, the recent realization that breaking the local symmetry could also drive formation of novel exotic phases, even when the global symmetry is preserved, has opened a new paradigm in materials design. In the specific case of inversion symmetry, local symmetry breaking can still lift the spin degeneracy through an asymmetry of the wavefunction, while bearing a zero net spin polarization [7, 8]. In this case, the resulting spin-locking pattern won't necessarily be in momentum, but could occur across different valleys [9] or layers [10].

The proposal of local symmetry breaking becomes even more appealing in the context of superconductivity, where it has been proposed that the effect could play a key role in determining which competing phases are stabilized, in favoring a specific symmetry of the superconducting order parameter, and ultimately even in enhancing the superconducting transition temperature [11]. Unconventional superconductors such as cuprates, pnictides, and even the recently reported 2D superconducting heterostructures [12–14] are particularly

attractive to study the interplay between spin-orbit coupling and superconductivity, as often the local symmetry breaking is intrinsic to their nature. In the case of cuprates and pnictides for example, short-range structural distortions and rotations of the octahedra [15, 16], and staggered stacking between layers [17], are all possible sources of local symmetry breaking, with the latter being also shared among the majority of 2D superconducting heterostructures [18]. In each one of these cases, it is therefore natural to expect that the details of the lattice symmetry are closely connected with spin-orbit coupling, which is an essential ingredient in the microscopic description and ultimately imprinted on the order parameter [11].

The level of sophistication that has been reached in measuring the spin-resolved electronic structure of materials [19], together with the recent report of a non-zero spin-momentum locking in centrosymmetric highly-overdoped cuprate superconductors [20], has opened a new frontier in this still poorly explored field. Here we use high resolution spin- and angle-resolved photoemission spectroscopy (spin-ARPES) to study the spin dependent electronic structure of cuprate superconductors as a function of momentum, doping, and family, spanning across both the electron- and hole-doped sides of the phase diagram.

We reveal the persistence of an intrinsic and universal spin texture in the Bi-based hole-doped side of the cuprate phase diagram, which becomes negligible on the electron-doped side. We attribute such spin asymmetry to a breaking of local inversion symmetry induced by the short range structural distortions of the CuO octahedra, and show how their reduction can lead to a suppression of the spin asymmetry. These findings reveal a never before seen connection between spin-orbit coupling and lattice symmetry with a clear imprint on the electronic structure, bringing forward the intriguing possibility that such interplay might be the missing key ingredient in understanding cuprate physics.

Four different cuprate samples - hole-doped double layer Bi2212 ($Bi_2Sr_2CaCu_2O_{8+x}$),

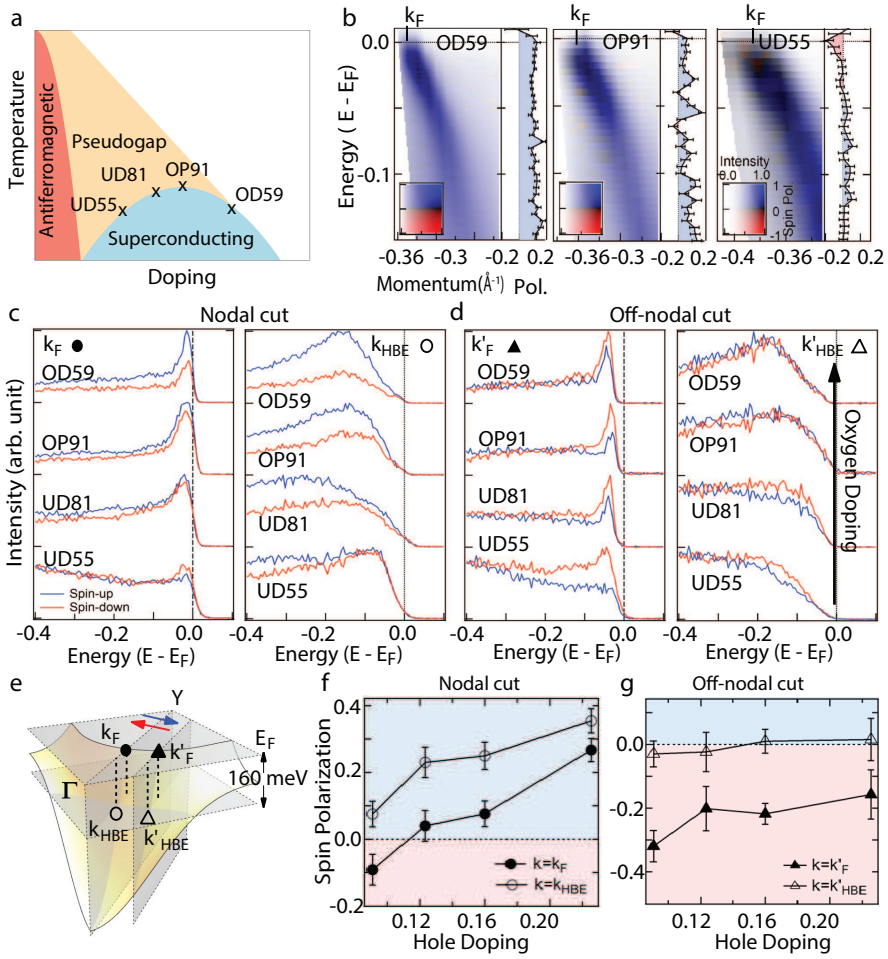

FIG. 1. **Doping dependent spin measurements of Bi2212. a)** Typical cuprate phase diagram. **b)** Spin-resolved nodal maps of UD55, OP91, and OD59. Color defines the spin polarization and brightness defines the intensity of the bands as shown in the inset. **c)**, **d)** Doping dependent spin-resolved energy distribution curves (EDCs) acquired at the Fermi level (k_F) and at higher binding energy (k_{HBE}, 160 meV below Fermi energy) along the **c)** nodal and **d)** off-nodal directions. All cuts are normalized to the OP sample quasiparticle peaks. **e)** Location of measured momenta in energy-momentum space. **f)**, **g)** Doping dependence of the total spin polarization at k_F (coherent peak) and k_{HBE} (incoherent humps).

single layer Bi2201 ($Bi_2Sr_2CuO_{6+x}$), lead-doped Bi2212 ($(Bi_{2-x}Pb_x)Sr_2CaCu_2O_{8+x}$) and electron-doped NCCO ($Nd_{2-x}Ce_xCuO_4$) - across several dopings were studied. Figure 1 shows the in-plane spin polarization across the nodal direction for double layer Bi2212 samples at four different dopings: underdoped (x = 0.091, T_c = 55 K (UD55), and x = 0.124, T_c = 81 K (UD81)), optimally doped (x = 0.16, T_c = 91 K (OP91)), and overdoped (x = 0.226, T_c = 59 K (OD59)) (panel a shows the location on a typical cuprate phase diagram). Data were collected with s-polarized light with the measured spin component in-plane and perpendicular to the nodal direction (Γ - Y), as schematically shown in panel e. Fig. 1b shows the 2-dimensional spin-resolved maps for some representative dopings (UD55, OP91, and OD59), where the color represents the direction of the spin polarization along the Fermi surface - blue is positive or "spin-up" and red is negative or "spin-down" as defined by the arrows in Fig. 1e, while the brightness shows the photoemission intensity. The spin-resolved nodal maps are mostly blue, suggesting that the spin-up channel is dominating. To the right of each map we show the strength of the spin polarization as a function of binding energy, defined as $P_y = (I_\uparrow - I_\downarrow)/(I_\uparrow + I_\downarrow)$, which reveals an overall decrease in magnitude, by approximately a factor of 3, from overdoped to underdoped.

To study in detail the doping dependence of the observed spin asymmetry, in Figure 1c,d we show the raw nodal and off-nodal energy distribution curves (EDCs) for the coherent quasiparticle peak at the Fermi momentum (k_F) and the incoherent peak at momentum k_{HBE}, corresponding to binding energy $E_B = 160$ meV. Two main results are observed as a function of doping. The first is a decrease of the total spin polarization from overdoped to underdoped for both coherent and incoherent quasiparticles; the second is the shift of spin polarization from positive to negative as a function of momentum, going from nodal to off-nodal directions (compare panels c and d). For the coherent quasiparticle peak at the node,

the positive spin polarization present in the overdoped sample decreases with less oxygen doping and eventually reverses to become negative for the heavily underdoped sample. The same negative trend persists for the incoherent part of the spectra, with an overall decrease of ∼25-30% for both momenta. Away from the nodal direction (Fig. 1d), a decrease in the spin polarization is still observed, but for both the coherent and the incoherent part of the spectra the total decrease is a lot smaller (∼3-13%). We note that since the polarization is doping dependent, spin asymmetry is an intrinsic property of the material rather than an extrinsic effect due a phase difference in the photoemission process [21], and represents a bulk property as will be discussed more in Figure 3.

In addition to the reversal of the direction of spin polarization as a function of doping and momentum, the overall magnitude of the polarization also shows an interesting doping dependence. Along the nodal direction (Fig. 1c), the spin-up channel shows stronger intensity with respect to the spin-down channel at both k_F and k_{HBE} for all dopings except for the underdoped sample. For the quasiparticle peak, the relative difference of the two spin channels decreases for both momenta and eventually reverses as the hole doping reduces. Fig. 1d shows that closer to the antinodal region, the quasiparticle peaks (k'_F) for all dopings have stronger negative spin intensity, with the most underdoped crystal showing the strongest difference. A similar pattern in the spin polarization can also be found at higher binding energy (k'_{HBE}). These behaviors are summarized in panels f and g, where we report the spin polarization of the quasiparticle peaks and incoherent humps as a function of doping. The data show a clear overall increase of the spin polarization direction as the oxygen doping level increases for both nodal and off-nodal directions, while the magnitude follows an opposite trend between the two directions.

To better visualize the momentum and doping dependence of the spin asymmetry, in

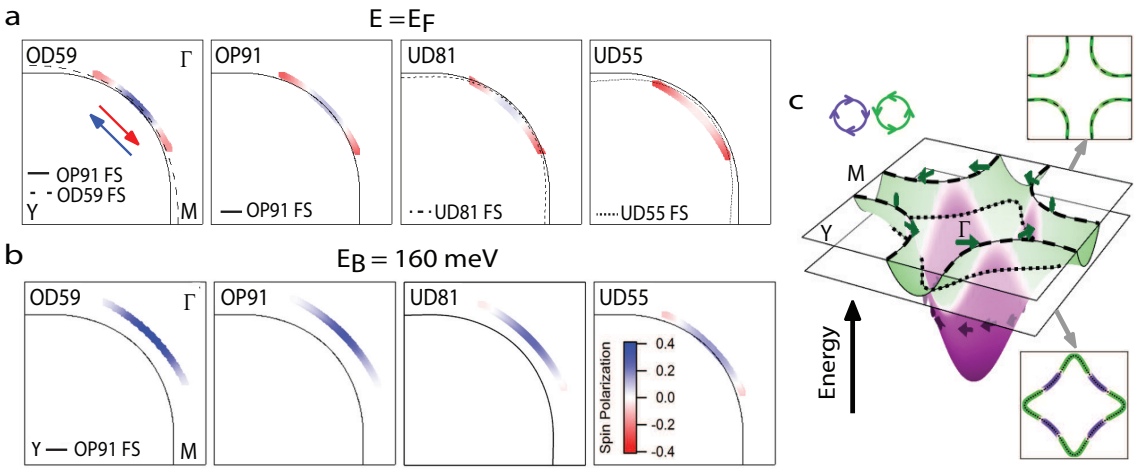

FIG. 2. **Doping dependence of spin-polarized Fermi surface and high binding energy maps of Bi2212 a)** Spin-polarized Fermi surface maps for the in-plane spin component, in one quadrant. **b)** Spin-polarized high binding energy maps. The solid black line in each panel represents the tight-binding Fermi surface at optimal doping, while the dashed lines are the calculated Fermi surface for overdoped to underdoped, as specified in each panel. **c)** Proposed 3D spin texture based on similarities between the polarization of OD59 in **a)** and UD55 in **b)** and their location in momentum space. The calculated band structure is colorcoded with respect to different spin helicity, with green representing counterclockwise helicity around Γ, and purple representing clockwise. The effect of changing the doping in a Bi2212 crystal is equivalent to taking a snapshot of spin in a fixed spin texture, so higher doping will yield spin with more clockwise helicity, and vice versa when decreasing the doping.

Figure 2 we report the doping dependence of the spin-polarized constant energy maps over one quadrant of the first Brillouin zone, at both E_F (Fermi surface, Fig. 2a) and at high binding energy (Fig. 2b). Calculated Fermi surfaces (FSs) based on a tight-binding model are also shown (dashed lines) for each doping level together with the calculated optimal doping Fermi level for comparison (solid lines). In addition to the standard decrease of

the hole-like Fermi surface with decreasing doping, we observe a gradual evolution of the spin polarization. Specifically in the overdoped regime, the polarization is positive along the Fermi arc and becomes negative as we move along the surface toward the antinode. The constant energy maps at high binding energy are mainly positive in the overdoped and optimally doped regime and gain some negative spin polarization in the underdoped regime toward the edge of the Fermi arc, reminiscent of the Fermi surface spin texture observed for higher doping (compare OD 59K Fermi surface map in Fig. 2a with UD 55K high energy map in Fig. 2b). These similarities, though from different peaks in the two samples (coherent vs incoherent), occur at momenta that are very close to each other as can be seen by the location of the constant energy maps in relation to the OP Fermi surface (see solid line). Therefore, the apparent complexity of the measured spin as a function of doping and binding energy can be reconciled by the presence of a spin texture shared between all doping levels where the observed spin polarization depends mainly on the momentum and energy of the photoelectron or in other words on the position of the chemical potential. Lowering the hole concentration (underdoped) raises the chemical potential, therefore changing the doping level is phenomenologically equivalent to taking snap shots at different binding energies of a three-dimensional fixed spin texture. This behavior is summarized in Fig. 2c where we schematically represent the 3D electronic band structure with the corresponding spin polarization, highlighting the presence of two different helicities - counterclockwise (green) and clockwise (purple) around Γ. This representation illustrates that the observed spin pattern manifests as rotations in the same (clockwise) direction around the Brillouin zone center and corners, instead of two competing spin textures circling the center.

To verify the intrinsic bulk nature of the observed spin texture and its proposed universality independent of doping, in Figure 3 we monitor the evolution of the spin dependent

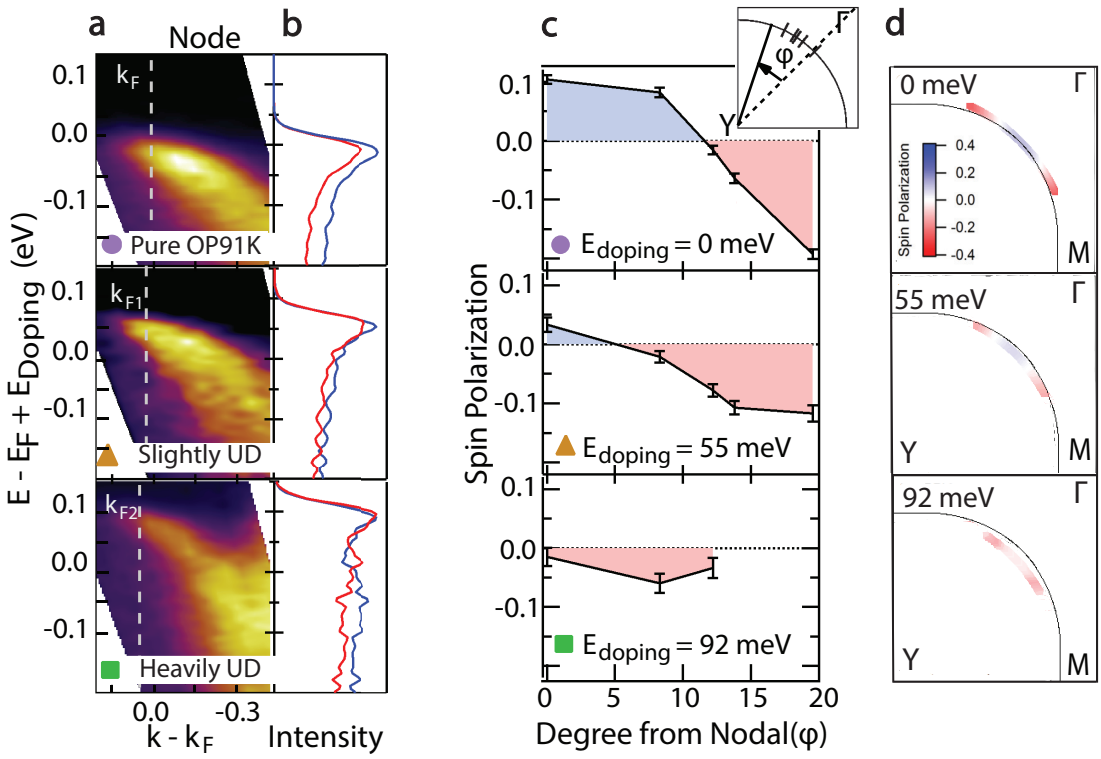

FIG. 3. **Potassium deposition on optimally doped Bi2212. a)** Spin-integrated nodal maps for different levels of potassium deposition. All three maps are adjusted by the Fermi momentum of the pure OP91 sample (k_F) for ease of comparison. k_{F1} and k_{F2} are the Fermi momenta for the slightly UD and heavily UD samples, respectively. **b)** Spin-resolved EDCs at k_F. E_F was raised ∼55 meV and ∼92 meV after the first and second deposition treatment, respectively. **c)** Spin polarization at k=k_F as a function of angle ϕ from the nodal direction (see inset) along the Fermi arc. **d)** Constant energy maps at the Fermi surface for comparison with Figure 2.

electronic structure while changing the chemical potential within the same sample. This is achieved via *in situ* doping through deposition of potassium (K) atoms on the cleaved surface of an optimally doped Bi2212 sample. Such an *in situ* doping method has been successfully used in ARPES to study the doping dependence of a variety of materials, from

2D systems [22] to cuprate superconductors [23]. In this case, potassium atoms donate electrons due to low ionization potential causing the exposed surface to lose holes (i.e. become more underdoped), which has an effect opposite to that of oxygen doping. Fig. 3a shows the spin-integrated nodal energy vs. momentum maps as a function of K doping. A clear rise in the chemical potential to 55 meV after the first K doping treatment and 92 meV after the second is observed, supporting the evolution of doping from optimal toward underdoped. The evolution of the corresponding spin-resolved EDC spectra are shown in panel b. The data reveal a decrease in the spin-up intensity toward underdoping similar to the doping dependence reported in Fig. 1. In Fig. 3c the full momentum dependence of the spin polarization is reported, showing that as the potassium content increases (the sample becomes more underdoped), the overall spin polarization at the node becomes more negative, with a decrease of $\sim$11% to 5% and then to -2% after the first and second deposition, respectively. By showing Fermi surface diagrams (Figure 3d) similar to those in Figure 2, we can compare the similarities between the spin textures at similar momenta. This reminiscence of the bulk oxygen doping dependence behavior reported in Figs. 1, 2 supports the universal intrinsic nature of the observed effect and its bulk origin in the Bi-based family.

To test the universality of the observed phenomena beyond double layer Bi2212, Figure 4 shows the momentum-dependent spin-resolved energy distribution curves for optimally-doped single layer Bi2201. Similarly to the double layer case, we observe a non-zero spin polarization along the nodal direction, with an overall decrease of the positive spin component moving away from the nodal direction, for both the coherent and incoherent peaks (Fig. 4a). Panel b shows the total spin polarization as a function of angle from the node, which matches the trend of the spin polarization in the double-layered cuprate from Figure 2.

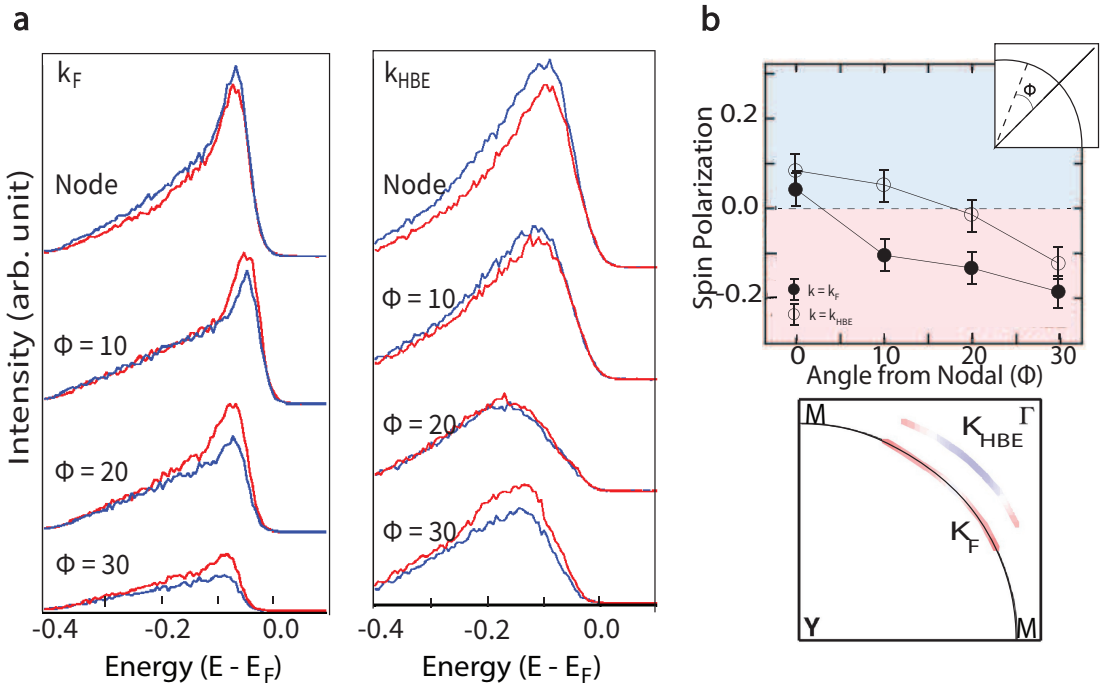

FIG. 4. **Spin polarization of single layer Bi2201 a)** Spin of single layer Bi2201 (T_C = 35 K) at the Fermi level (left) and at the incoherent hump (right). **b)** Total spin polarization at k_F (coherent peak) and k_{HBE} (incoherent humps) along the Fermi surface.

The results presented here add two important pieces of information with respect to previous work. The first one points to the existence of the spin asymmetry beyond the double-layer overdoped Bi2212 and its persistence over the entire phase diagram and in other Bi-based compounds; the second one asks for a local electric field, different from the previously discussed lack of an inversion center on the CuO_2 planes within the same unit cell [20]. While this mechanism can be responsible for the out of plane electric field in the double layer case, it cannot account for the electric field in the single layer case where the CuO_2 plane is inversion symmetric (see SI). Clearly a different and universal source of electric field is needed.

Here we propose that such a field derives from the local structural fluctuations of the CuO

octahedra, a common feature of p-type cuprates including La- [15, 24, 25], Bi- [26–28], Hg- [29], Tl- [30], and Y- [31] based families, which is also responsible for charge inhomogeneity. These distortions, caused by the misfit strain between the CuO_2 plane and the rocksalt layers [25, 32], lead to tilting of the CuO_2 planes along the (110) and (010) direction, and the formation of local domains with orthorombic (LTO) and tetragonal (LTT) structure [15, 16], resulting in anharmonic incommensurate modulations and inhomogeneous lattice and charge [24, 27, 33]. In each plane only half of all Cu-O-Cu bonds are buckled, so these tiltings lead to a local symmetry breaking within an individual plane, while the overall fourfold symmetry and the average structure are preserved [26]. This newly proposed source of field gives a Rashba-like spin texture similar to the one previously considered [20], and hence is able to account for the observation here reported.

A direct way to test this proposal is to study the spin dependent electronic structure upon the removal of these local structural distortions. This situation is naturally achieved in the electron-doped cuprates like NCCO, where the CuO_2 planes have been reported to be mostly homogeneous. On the other hand, a way to achieve a more controlled removal of these distortions is by leveraging the widely studied superstructure along the (110) direction in the BiO plane of double layer Bi2212 [34], which is directly linked to the local structural fluctuations of the CuO_2 planes [26–28], and is a consequence of the release of the misfit strain. Upon partial substitution of Pb^{2+} ions in place of smaller Bi^{3+} in Bi2212 the amplitude of the superstructure decreases, eventually disappearing with high Pb concentrations [35].

These two situations are studied in Figure 5, where we report the spin dependent electronic structure at k_F of Pb-doped Bi2212 (overdoped, $T_C = 64$ K) and electron-doped cuprate $Nd_{2-x}Ce_xCuO_4$ (NCCO). The local lattice fluctuations are strongly reduced for the

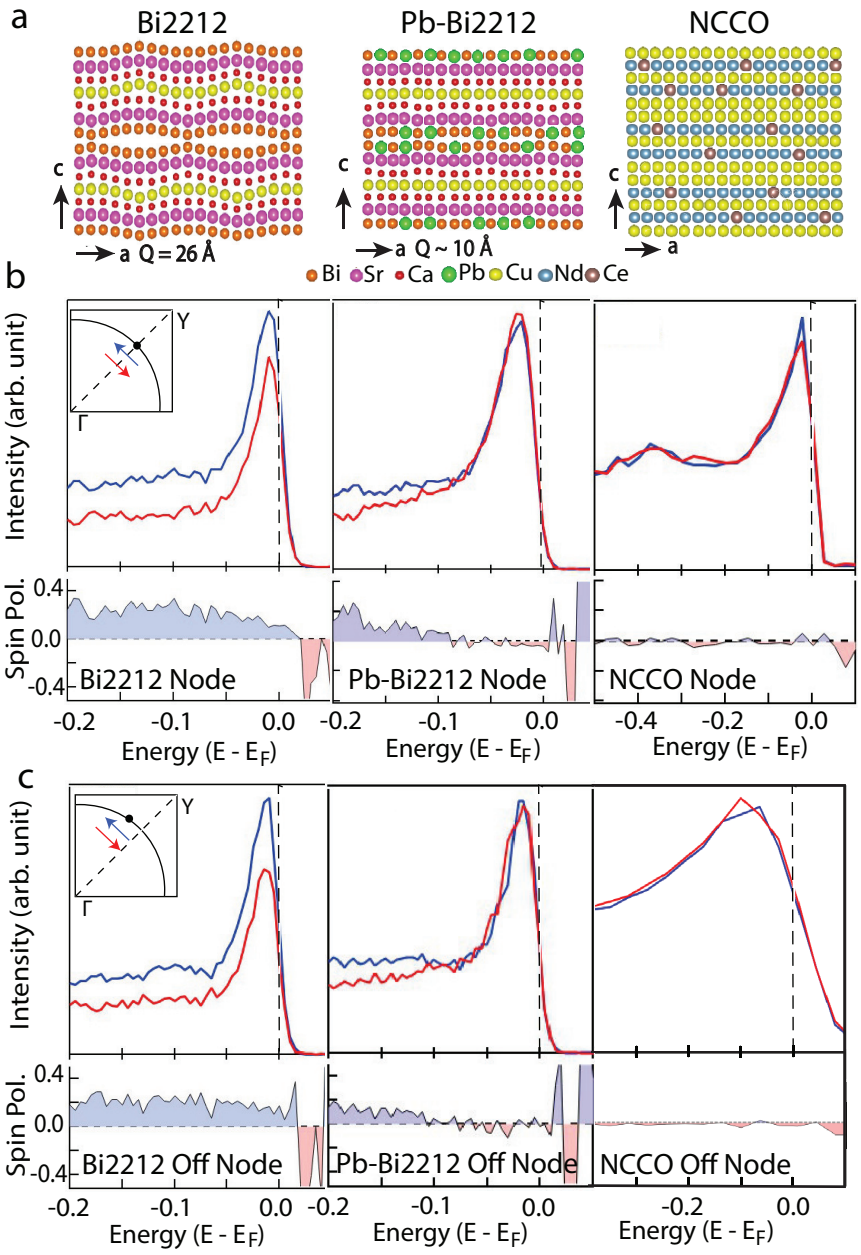

FIG. 5. **Suppression of spin polarization in Pb-doped Bi2212 and electron-doped NCCO** **a)** Cartoon depiction of the out-of-plane incommensurate distortion in OD Bi2212, OD Pb-Bi2212, and NCCO respectively. **b)** Spin-resolved EDCs and polarization of the spin component perpendicular to Γ-Y measured at k_F along the nodal direction and **c)** off-nodal direction (see inset) for all three samples.

first and almost absent for the latter. The relative EDC spectra at the node and off-node are shown with respect to the spin polarization. A striking reduction of the spin polarization is observed in the coherent part of the spectra for the Pb-doped sample, with respect to Bi2212, with the imbalance of the spin-up and spin-down intensities completely diminished. This is overall consistent with the proposed model where the spin asymmetry is driven by the local lattice modulation. Interestingly, the suppression of the spin asymmetry appears to occur only in the coherent part of the spectra (quasiparticle peak), while it is only weakly affected at higher energy (incoherent part). Whether this is due to some more complex mechanism than the one presented here or is a remnant effect due, for example, to the Pb-induced disorder, it is clear that further studies are needed to better understand the origin of this non-trivial energy dependence.

Similarly, in the case of electron-doped NCCO, the nodal spin-resolved EDCs at k_F show an almost negligible spin polarization. This observation further supports the proposed scenario where the driving dipole field that leads to non-zero SOC is induced by local lattice fluctuations, which are common to all hole-doped cuprates, as previously discussed, but almost absent in electron-doped ones. This observation brings forward the intriguing possibility that the unsolved phase diagram asymmetry between electron- and hole-doped cuprates might be a consequence of spin-orbit coupling. It is clear that a continued investigation of how effectively SOC can lift the spin degeneracy of other electron- and hole-doped cuprate families and their doping dependence is needed to substantiate this possibility.

In summary, the results shown here demonstrate the effect of local lattice fluctuations and consequent local symmetry breaking in driving a universal and intrinsic spin-orbit coupling in hole-doped Bi-based cuprates. Recent theoretical works have proposed that SOC could play an important role in cuprate physics, by stabilizing, for example, the onset of a metallic

phase out of an antiferromagnetic insulating background, as recently shown in the case of a Hubbard plaquette [36], or by enhancing the formation of a charge density wave (CDW) and pseudogap phase [37], ferromagnetic ordering [38, 39], and even superconductivity [40], in effect turning on different components for the symmetry of the order parameter [11]. In the underdoped regime, d-density wave [41] and loop-current order [42] models used to describe the pseudogap phase, both rely on a non-zero SOC that couples the orbital current with the spin channel. In addition, SOC may play a role in the development of pair density wave, which could be an alternative and competing ground state to d-wave superconductivity in cuprates, via local inversion asymmetry [43]. Moreover, it has been shown that this mutual interplay between SOC and local lattice fluctuations might also have important consequences in defining the shape of the energy landscape, eventually favoring a "Mexican hat" energy surface over a parabolic one in the limit of strong SOC [44]. Although many of these predictions require further experimental investigations and the purpose of the present work is not to justify any of them, the results presented here demonstrate the importance of including lattice spin-orbit coupling interplay in any theory for superconductivity to examine the role it might play in stabilizing the underlying ground state and to understand how different phases intertwine and ultimately define the emerging symmetry of the order parameter. For example, the recent discovery of superconductivity in 2D heterostructures [12], where lattice-driven local symmetry breaking and its periodicity, strain, and SOC [45] can be easily tuned via stacking or twisting, gives rise to the idea of methodically studying how SOC and lattice symmetry affects the order parameter. At the same time, this study can inform on new ways to engineer novel spin-orbit coupled superconductors where the imprint of SOC on the order parameter acts as a booster of the superconducting transition [11]. Finally, since similar local symmetry breaking due to either a local rotation or tilting of

the octahedra structure have been reported in other correlated materials such as pnictides, iridates, ruthenates, and manganites [46–49] with similar structural characteristics, non-zero SOC, and complex phase diagrams, the present work suggests that mutual interplay between SOC and local lattice fluctuations might play a more universal role in driving the unusual properties of correlated materials and unconventional superconductivity beyond cuprate physics.

I. METHODS

Single crystal hole-doped $Bi_2Sr_2CaCu_2O_{8+x}$ and $Bi_2Sr_2CuO_{6+x}$ samples grown by the floating zone method were cleaved at temperature $\approx$ 30 K in ultrahigh vacuum chamber under $\approx 5 \times 10^{-11}$ Torr, except for UD55, which was measured at $\approx$ 90K. Previous measurements have shown that the spin remains the same above and below T_C. Single crystal NCCO ($Nd_{2-x}Ce_xCuO_4$) samples with x = 0.145 were measured in ultrahigh vacuum at $\approx$ 20 K on a table top 11 eV system (Fig. 5b), and at 80 eV at Beamline 10.0.1.2 at the ALS (Fig. 5c). The critical temperature of each sample is given in the main text. The samples were probed with 5.99 eV photons produced by two stages of second harmonic generation from the output of a Ti:sapphire oscillator. The data in the present work were acquired with a time-of-flight spectrometer utilizing an exchange-based spin polarimeter with energy and momentum resolution $\Delta E \approx 15$ meV and $\Delta k \approx \pm 0.02$ Å^{-1}, respectively [50]. The spin-resolved nodal map of UD50 in Fig. 1(b) was taken with a larger aperture, yielding momentum resolution ± 0.08 Å^{-1}.

ACKNOWLEDGMENTS

We thank D. H. Lee, A. Vishwanath, M. Serbyn, and E. Altman for very insightful discussions. **Funding:** This work was primarily supported by the Lawrence Berkeley National Laboratory Ultrafast Materials Sciences program, funded by the U.S. Department of Energy, Office of Science, Office of Basic Energy Sciences, Materials Sciences and Engineering Division, under contract DE-AC02-05CH11231. This research used resources of the Advanced Light Source, which is a DOE Office of Science User Facility under contract DE-AC02-05CH11231. The work at the University of Minnesota was funded by the U.S. Department of Energy through the University of Minnesota Center for Quantum Materials, under Grant No. DE-SC0016371 **Author Contributions:** K.C., C.Y.L., and K.G. carried out the experiments. BSCCO samples were prepared by H.E. NCCO samples were prepared in M.G.'s lab. A.L. was responsible for experimental planning, infrastructure, and experimental design. The manuscript was written by K.C. and A.L., with input from all other authors. **Competing interests:** The authors declare no competing financial interests. **Data and materials availability:** All data are available in the manuscript.

---

[1] Enquist, M. & Arak, A. Symmetry, beauty, and evolution. *Nature* **372**, 169–172 (1994). URL https://doi.org/10.1038/372169a0.

[2] Landau, L. D. On the theory of phase transitions. *Zh. Eksp. Teor.* **7**, 19–32 (1937). URL http://archive.ujp.bitp.kiev.ua/files/journals/53/si/53SI08p.pdf.

[3] Bauer, E. & Sigrist, M. Non-Centrosymmetric Superconductors: Introduction and Overview. (Springer, Heidelberg, 2012) URL https://www.springer.com/gp/book/9783642246234.

[4] Smidman, M., Salamon, M. B., Yuan, H. Q. & Agterberg, D. F. Superconductivity and spin-orbit coupling in noncentrosymmetric materials: a review. *Rep. Prog. Phys.* **80**, 036501 (2017). URL https://doi.org/10.1088/1361-6633/80/3/036501.

[5] Gorkov, L. P. & Rashba, E. I. Superconducting 2D system with lifted spin degeneracy: Mixed singlet-triplet state. *Phys. Rev. Lett.* **87**, 037004 (2001). URL https://doi.org/10.1103/PhysRevLett.87.037004.

[6] Frigeri, P. A., Agterberg, D. F., Koga, A. & Sigrist, M. Superconductivity without Inversion Symmetry: MnSi versus $CePt_3Si$. *Phys. Rev. Lett.* **92**, 097001 (2004). URL https://doi.org/10.1103/PhysRevLett.92.097001.

[7] Zhang, X. *et al.* Hidden spin polarization in inversion-symmetric bulk crystals. *Nature Physics* **10**, 387–393 (2014). URL http://dx.doi.org/10.1038/nphys2933.

[8] Yuan, L. *et al.* Uncovering and tailoring hidden Rashba spin-orbit splitting in centrosymmetric crystals. *Nature Communications* **10**, 906 (2019). URL https://doi.org/10.1038/s41467-019-08836-4.

[9] Bawden, L. *et al.* Spin-valley locking in the normal state of a transition-metal dichalcogenide superconductor. *Nature Communications* **7**, 11711 (2016). URL https://doi.org/10.1038/ncomms11711.

[10] Yao, W. *et al.* Direct observation of spin-layer locking by local Rashba effect in monolayer semiconducting $PtSe_2$ film. *Nature Communications* **8**, 14216 (2017). URL http://dx.doi.org/10.1038/ncomms14216.

[11] Fischer, M. H., Loder, F. & Sigrist, M. Superconductivity and local noncentrosymmetricity in crystal lattices. *Phys. Rev. B* **84**, 184533 (2011). URL https://link.aps.org/doi/10.1103/PhysRevB.84.184533.

[12] Cao, Y. *et al.* Unconventional superconductivity in magic-angle graphene superlattices. *Nature* **556**, 43–50 (2018). URL https://doi.org/10.1038/nature26160.

[13] Bozovic, I. Atomic-layer engineering of superconducting oxides: Yesterday, Today, Tomorrow. *IEEE Transactions on Applied Superconductivity* **11**, 1 (2001). URL https://doi.org/10.1109/77.919617.

[14] Reyren, N. *et al.* Superconducting Interfaces Between Insulating Oxides. *Science* **317**, 5842 (2007). URL https://doi.org/10.1126/science.1146006.

[15] Bianconi, A. *et al.* Determination of the Local Lattice Distortions in the CuO_2 Plane of $La_{1.85}Sr_{0.15}CuO_4$. *Phys. Rev. Lett.* **76**, 3412–3415 (1996). URL https://link.aps.org/doi/10.1103/PhysRevLett.76.3412.

[16] Billinge, S., Kwei, G. H. & Tagaki, H. Local octahedral tilts in $La_{2-x}Ba_xCuO_4$: evidence for a new structural length scale. *Phys. Rev. Lett.* **72**, 2282 (1994). URL https://doi.org/10.1103/PhysRevLett.72.2282.

[17] Sigrist, M. *et al.* Superconductors with staggered non-centrosymmetricity. *J. Phys. Soc. Jpn.* **83**, 061014 (2014). URL https://doi.org/10.7566/JPSJ.83.061014.

[18] Du, L. *et al.* Engineering symmetry breaking in 2D layered materials. *Nature Reviews Physics* **3**, 193–206 (2021). URL https://doi.org/10.1038/s42254-020-00276-0.

[19] Lin, C.-Y., Moreschini, L. & Lanzara, A. Present and future trends in spin-ARPES. *Europhysics Letters* **134**, 57001 (2021). URL https://doi.org/10.1209/0295-5075/ac0c87.

[20] Gotlieb, K. *et al.* Revealing hidden spin-momentum locking in a high-temperature cuprate superconductor. *Science* **362**, 1271–1275 (2018). URL https://doi.org/10.1126/science.aao0980.

[21] Fanciulli, M. *et al.* Spin polarization and attosecond time delay in photoemission from spin degenerate states of solids. *Phys. Rev. Lett.* **118**, 067402 (2017). URL https://link.aps.org/doi/10.1103/PhysRevLett.118.067402.

[22] Zhou, S. Y., Siegel, D. A., Fedorov, A. V. & Lanzara, A. Metal to insulator transisiton in epitaxial graphene induced by molecular doping. *Phys. Rev. Lett.* **101**, 086402 (2008). URL https://doi.org/10.1103/PhysRevLett.101.086402.

[23] Hossain, M. A. *et al.* In situ doping control of the surface of high-temperature superconductors. *Nature Physics* **4**, 527–531 (2008). URL http://dx.doi.org/10.1038/nphys998.

[24] Bozin, E. O. *et al.* Neutron Diffraction Evidence of Microscopic Charge Inhomogeneities in the CuO_2 Plane of Superconducting $La_{2-x}Sr_xCuO_4$ ($0 \leq x \leq 0.30$). *Phys. Rev. Lett.* **84**, 5856–5859 (2000). URL https://link.aps.org/doi/10.1103/PhysRevLett.84.5856

[25] Billinge, S. & Duxbury, P. M. Structural compliance, misfit strain and stripe nanostructures in cuprate superconductors. *Phys. Rev. B* **66**, 064529 (2002). URL https://doi.org/10.1103/PhysRevB.66.064529.

[26] Bianconi, A. *et al.* Stripe structure of the CuO_2 plane in $Bi_2Sr_2CaCu_2O_{8+y}$ by anomalous x-ray diffraction. *Phys. Rev. B* **54**, 4310–4314 (1996). URL https://link.aps.org/doi/10.1103/PhysRevB.54.4310.

[27] Slezak, J. A., Lee, Jinho, Wang, M., & Davis, J. C. Imaging the impact on cuprate superconductivity of varying the interatomic distances within individual crystal unit cells. *Proc. Natl. Acad. Sci. U. S. A.* **105**, 9 (2008). URL https://doi.org/10.1073/pnas.0706795105.

[28] Saini, N. L., Lanzara, A, Bianconi, A., & Oyanagi, H. Local structural features of the superconducting $Bi_2Sr_2CaCu_2O_{8+\delta}$ system: A polarized Cu K-edge XAS study. *Phys. Rev. B* **58**, 11768 (1998). URL https://doi.org/10.1103/PhysRevB.58.11768

[29] Lanzara, A. *et al.* Anomalous local atomic correlations in $HgBa_2CuO_{4+\delta}$. *Phys. Rev. B* **59**, 3851 (1999). URL https://doi.org/10.1103/PhysRevB.59.3851.

[30] Pelc, D. *et al.* Unconventional short-range structural fluctuations in cuprate high T_C superconductors. *Preprint* URL https://arxiv.org/abs/2103.05482.

[31] Mustre De Leon, J., Conradson, S. D., Bastistić, I. & Bishop, A. R. Evidence for an Axial Oxygen-Centered Lattice Fluctuation Associated with the Superconducting Transition in $YBa_2Cu_3O_7$. *Phys. Rev. Lett.* URL https://doi.org/10.1103/PhysRevLett.65.1675.

[32] Di Castro, D. *et al.* Evidence for the strain critical point in high T_C superconductors. *Eur. Phys. J. B* **18**, 617-624 (2000). URL https://doi.org/10.1007/s100510070010.

[33] Mihailović, E., Ruani, G., Kaldis, E. & Müller, K. A. Anharmonic Properties of High-T_C Cuprates. (World Scientific, 1995) URL https://doi.org/10.1142/9789814533065.

[34] Gao, Y. *et al.* The incommensurate modulation of the 2212 Bi-Sr-Ca-Cu-O superconductor. *Science* **241**, 954–956 (1988). URL https://doi.org/10.1126/science.241.4868.954.

[35] Liu, J. *et al.* Evolution of incommensurate superstructure and electronic structure with Pb substitution in $(Bi_{2-x}Pb_x)Sr_2CaCu_2O_{8+\delta}$ superconductors. *Chinese Phys. B* **28**, 077403 (2019). URL https://doi.org/10.1088/1674-1056/28/7/077403.

[36] Brosco, V. & Guerci, D. & Capone, M. Pauli metallic ground state in Hubbard clusters with Rashba spin-orbit coupling. *Phys. Rev. B* **97**, 125103 (2018). URL https://link.aps.org/doi/10.1103/PhysRevB.97.125103

[37] Lu, X. & Senechal, D. Spin texture in a bilayer high-temperature cuprate superconductor. *Phys. Rev. B* **104**, 024502 (2021). URL https://doi.org/10.1103/PhysRevB.104.024502.

[38] Matzdorf, R. *et al.* Ferromagnetism stabilized by lattice distortion at the surface of the p-wave superconductor Sr_2RuO_4. *Science* **289**, 746–748 (2000). URL https://doi.org/10.1126/

science.289.5480.746.

[39] Kopp, A. *et al.* Competing ferromagnetism in high-temperature copper oxide superconductors. *Proc. Natl. Acad. Sci. U. S. A.* **104**, 6123–6127 (2007). URL https://doi.org/10.1073/pnas.0701265104.

[40] Hurand, S. *et al.* Field-effect control of superconductivity and Rashba spin-orbit coupling in top-gated $LaAlO_3/SrTiO_3$ devices. *Scientific Reports* **5**, 12751 (2015). URL https://doi.org/10.1038/srep12751.

[41] Wu, C., Zaanen, J., & Zhang, S.-C. Spin-orbit coupling-induced magnetic phase in the *d*-density-wave phase of $La_{2-x}Ba_xCuO_4$ superconductors. *Phys. Rev. Lett.* **95**, 247007 (2005). URL https://doi.org/10.1103/PhysRevLett.95.247007.

[42] Aji, V. & Varma, C. M. Spin order accompanying loop-current order in cuprate superconductors. *Phys. Rev. B* **75**, 224511 (2007). URL https://link.aps.org/doi/10.1103/PhysRevB.75.224511.

[43] Yoshida, T., Sigrist, M. & Yanase, Y. Pair-density wave states through spin-orbit coupling in multilayer superconductors. *Phys. Rev. B* **86**, 134514 (2012). URL https://link.aps.org/doi/10.1103/PhysRevB.86.134514.

[44] Streltsov, S. & Khomskii, D. Jahn-Teller effect and spin-orbit coupling: friends or foes?. *Phys. Rev. X* **10**, 031043 (2020). URL https://link.aps.org/doi/10.1103/PhysRevX.10.031043.

[45] Ernandes, C. *et al.* Strain and spin-orbit coupling engineering in twisted WS_2/graphene heterobilayer. *Nanomaterials* **11** (11), 2921 (2021). URL https://doi.org/10.3390/nano11112921.

[46] Caivano, R. *et al.* Feshbach resonance and mesoscopic phase separation near a quantum critical point in multiband FeAs-based superconductors. *Supercond. Sci. Technol.* **22**, 014004 (2009). URL https://doi.org/10.1088/0953-2048/22/1/014004.

[47] Yanase, Y. Random spin-orbit coupling in spin-triplet superconductors: stacking faults in Sr_2RuO_4 and $CePt_3Si$. *J. Phys. Soc. Jpn.* **79**, 084701 (2010). URL https://doi.org/10.1143/JPSJ.79.084701.

[48] Lanzara, A. *et al.* Crossover from large to small polarons across metal-insulator transition in manganites. *Phys. Rev. Lett.* **81**, 878 (1998). URL https://doi.org/10.1103/PhysRevLett.81.878.

[49] Subramanian, M. A. *et al.* Sr_2RhO_4 and Sr_2IrO_4: Structural and magnetic studies of 4d and 5d transition metal analogs of La_2CuO_4. *Physica C: Superconductivity* **235–240**, 743–744 (1994). URL https://doi.org/10.1016/0921-4534(94)91596-2.

[50] Jozwiak, C. *et al.* A high-efficiency spin-resolved photoemission spectrometer combining time-of-flight spectroscopy with exchange-scattering polarimetry. *Rev. Sci. Instrum.* **81**, 053904 (2010). URL https://doi.org/10.1063/1.3427223.

EXTENDED DATA

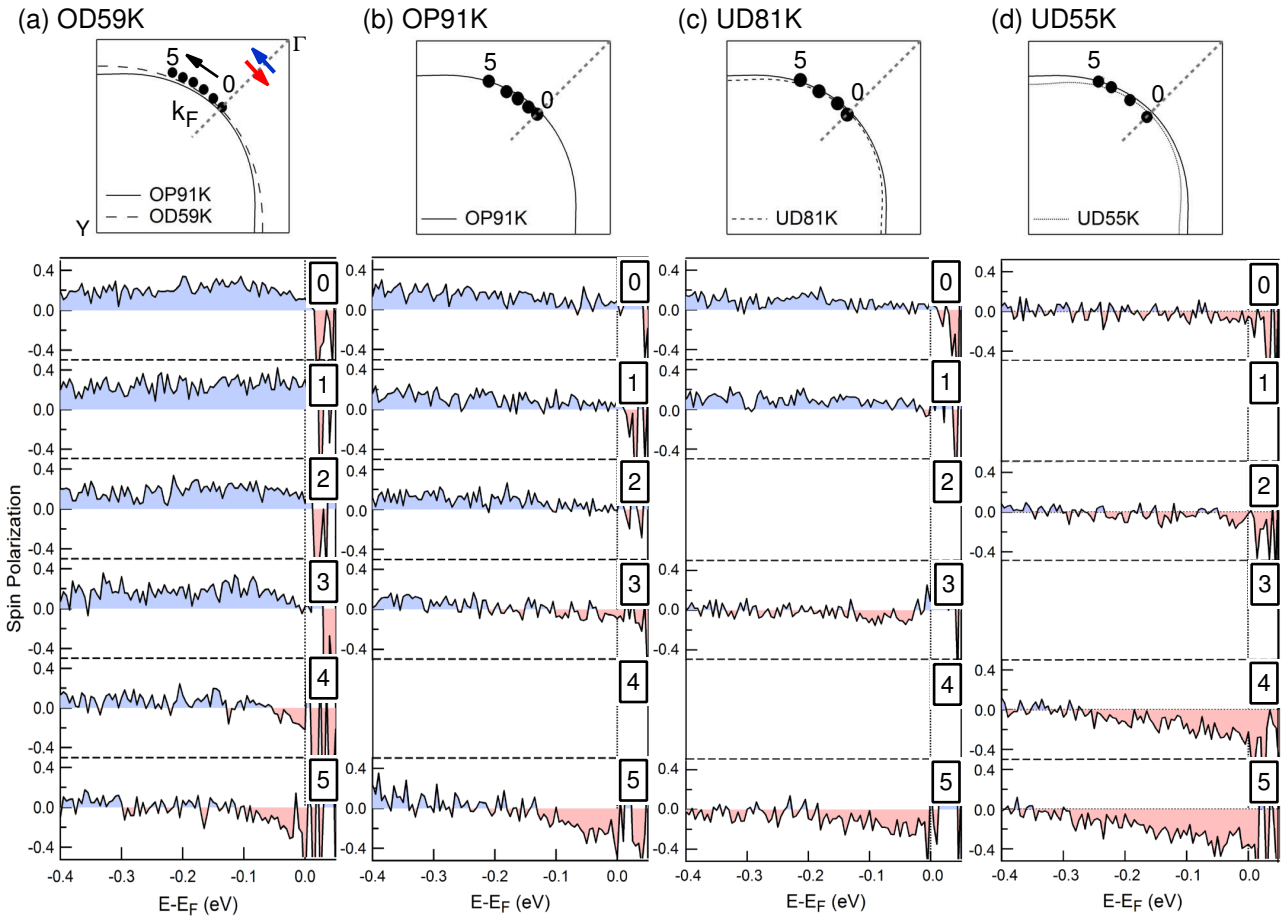

FIG. 6. Momentum dependence of spin polarization at the Fermi energy. The measured spin component is perpendicular to nodal direction as described in the main text. The polarization curves are taken at the momentum denoted with solid circles.

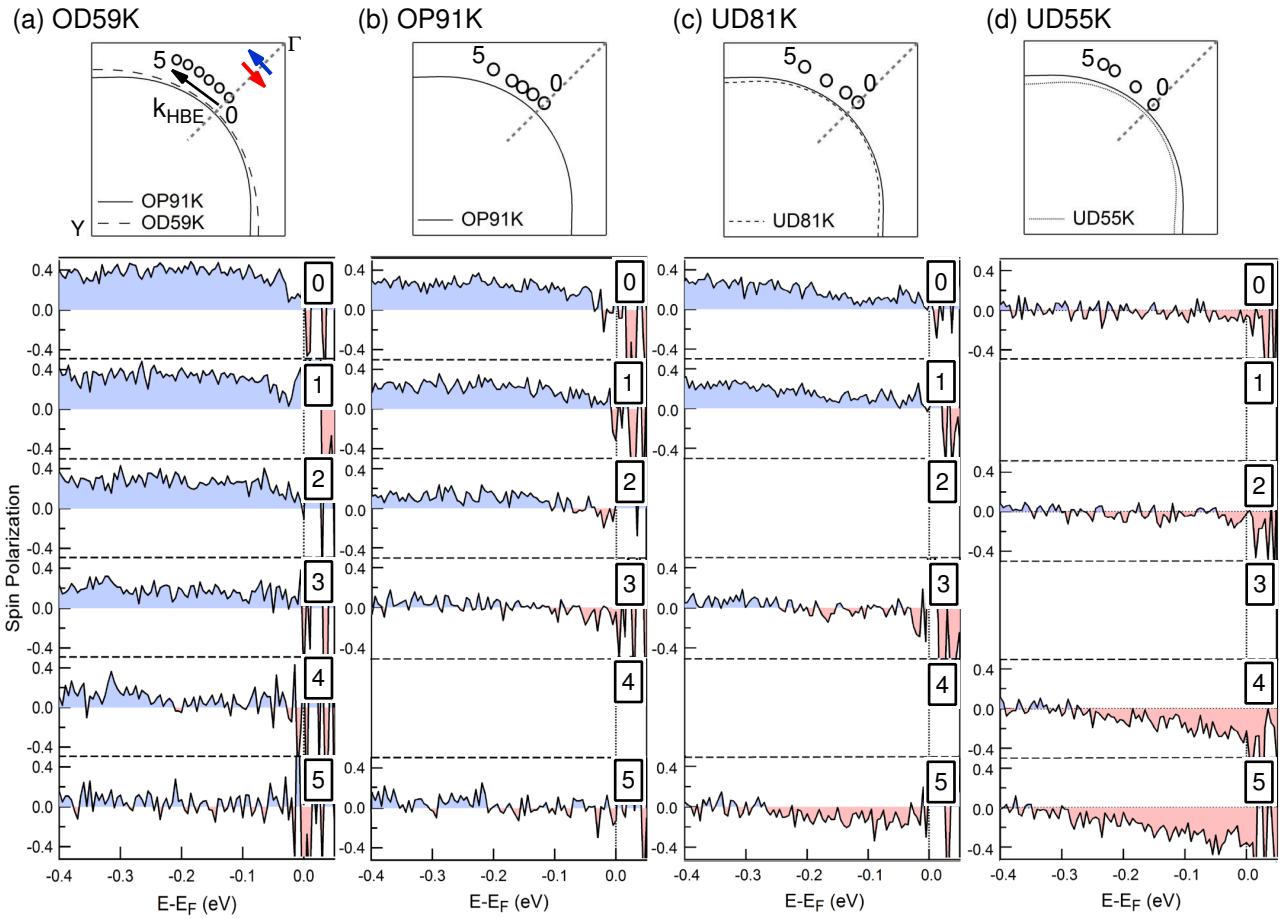

FIG. 7. Momentum dependence of spin polarization at incoherent peaks (E_B=160 meV). The polarization curves are taken at the momentum denoted with open circles.